Simulation Studies for an Urban Air Mobility Aircraft using Hardware-In-Loop Experiments

Chetan S. Kulkarni *
KBR Inc, NASA Ames Research Center, Moffett Field, CA, 94035, USA.

Priyank Pradeep †
Universities Space Research Association, NASA Ames Research Center, Moffett Field, CA, 94035, USA.

Gano B. Chatterji ‡
Crown Consulting, Inc., NASA Ames Research Center, Moffett Field, CA, 94035, USA.

Urban Air Mobility seeks to transport passengers, deliver cargo, and provide emergency medical transportation in major metropolitan areas. This will be accomplished with distributed electric powered vertical takeoff and landing aircraft. The low specific energy of the current generation lithium-ion battery packs limit the operational range of the electric aircraft. Limited range impacts safety by reducing the amount of time available for analyzing the potential impact of errors and failures and responding to them, and for flying to an alternative landing area or returning to the base. It is therefore critical to understand the impact of flight and environmental conditions on the onboard lithium-ion battery pack's health. With this as the motivation, the procedure for evaluating the performance of battery packs in a laboratory setting and the results obtained using this procedure on battery packs subject to power draw characteristics of a simulated flight of a NASA conceptual multirotor aircraft model are described. The fully charged battery is allowed to discharge at specific C-rates based on the power draw profile during the experiment, and the current and voltages are recorded as a function of time. Observed results under different operating conditions and mission profiles are discussed.

I. Nomenclature

D	=	Parasite drag
T	=	Net thrust
T_{rotor}	=	Thrust produced by an isolated rotor
C_{T}	=	Thrust coefficient
λ	=	Latitude of the aircraft
τ	=	Longitude of the aircraft
h	=	Altitude above mean sea level of the aircraft
n	=	Number of rotors installed on the aircraft
v_h	=	Rotor induced velocity in hover
v_i	=	Rotor induced velocity during forward flight
V	=	True airspeed of the aircraft
V_l	=	Lateral component of the true airspeed of the aircraft
V_v	=	Vertical component of the true airspeed of the aircraft
V_{GS}	=	Groundspeed of the aircraft
m	=	Mass of the aircraft
I_i	=	Moment of inertia of the i^{th} rotor
q	=	Dynamic pressure on the aircraft
ρ	=	Density of air
W_e	=	East component of wind velocity

*Research Scientist, KBR Inc, NASA Ames Research Center, AIAA Associate Fellow.
†Aerospace Engineer, Universities Space Research Association, NASA Ames Research Center, AIAA Senior Member.
‡Senior Scientist and Lead, Crown Consulting Inc., NASA Ames Research Center, AIAA Associate Fellow.

W_n	=	North component of wind velocity
W_v	=	Vertical (up) component of wind velocity
α	=	Angle of attack of air-stream relative to rotor tip path plane
γ	=	Aerodynamic flight path angle of the aircraft
ψ	=	Heading angle of the aircraft
χ	=	Course angle of the aircraft
θ	=	Rotor tip-path-plane pitch angle
ϕ	=	Rotor tip-path-plane roll angle
κ	=	Induced power factor
P_{max}	=	Total maximum deliverable power
P_{req}	=	Instantaneous power required in forward flight
P_{battery}	=	Instantaneous power supplied by the onboard lithium-ion polymer battery pack
A_{rotor}	=	Rotor disk area
R	=	Radius of the rotor
R_{Earth}	=	Radius of the Earth assuming spherical model
ω	=	Rotational speed of the rotor blades
σ	=	Thrust weighted solidity ratio
$C_{\text{d mean}}$	=	Mean blade drag coefficient
Li-Po	=	Lithium-ion polymer battery
SOC	=	State-of-charge of the onboard lithium-ion polymer battery pack
EOD	=	End-of-discharge of the onboard lithium-ion polymer battery pack
V(t)	=	Voltage of the onboard lithium-ion polymer battery pack

II. Introduction

Recent technological advances have made it possible to build and flight test electric Vertical Takeoff and Landing (eVTOL) aircraft [1–3]. Several companies such as Airbus A^3, Aurora Flight Sciences, EHang, Joby Aviation, Kitty Hawk, Leonardo, Lilium, Terrafugia and Volocopter are developing different types of eVTOL aircraft [3]. They all employ distributed electric propulsion (DEP) systems [2]. The low specific energy of current lithium-ion polymer (Li-Po) battery technology used for powering DEP system constrains the range of flight. Limited range has safety impact due to the reduced amount of time available for the pilot to assess the situation and take corrective actions, and for flying to an alternative landing area or returning to the origin in emergency situations. An important area of research therefore is accurate prediction of the state of the onboard Li-Po battery pack for safety margin assessment for continuation of the mission or for invoking contingencies.

This work integrates the computed power demand obtained from the trajectory simulation of a quad-rotor vehicle model into a hardware-in-the-loop test with the battery pack for observing the battery discharge characteristics. The power demand values obtained from the trajectory simulation are normalized to a 6S-22Ah battery pack for performing the hardware-in-the-loop experiments.The 6S-22Ah battery pack has six cells connected in series, and the load connected to it can draw 22A for an hour.

The paper is organized as follows. Section III discusses the fight dynamics and kinematics of the quad-rotor vehicle and the power consumption model. This section also briefly outlines the procedure for simulating the horizontal and vertical trajectories using the aircraft performance model and the equations-of-motion. The power consumption model provides the power required for flying the trajectory as a function of time. Section IV describes normalization of power consumption values to enable testing with a smaller battery pack and the setup for hardware-in-the-loop testing. Section V presents the test results and their analysis. Finally, the conclusions and future work are discussed in Section VI.

III. Aircraft Trajectory Simulation for Power Demand

In this research, a quadrotor eVTOL aircraft concept model proposed by Silva et al. [4], shown in Figure 1a, is used to estimate power consumption. Li-po (Lithium polymer) battery packs are subject to this estimated power draw in experiments.

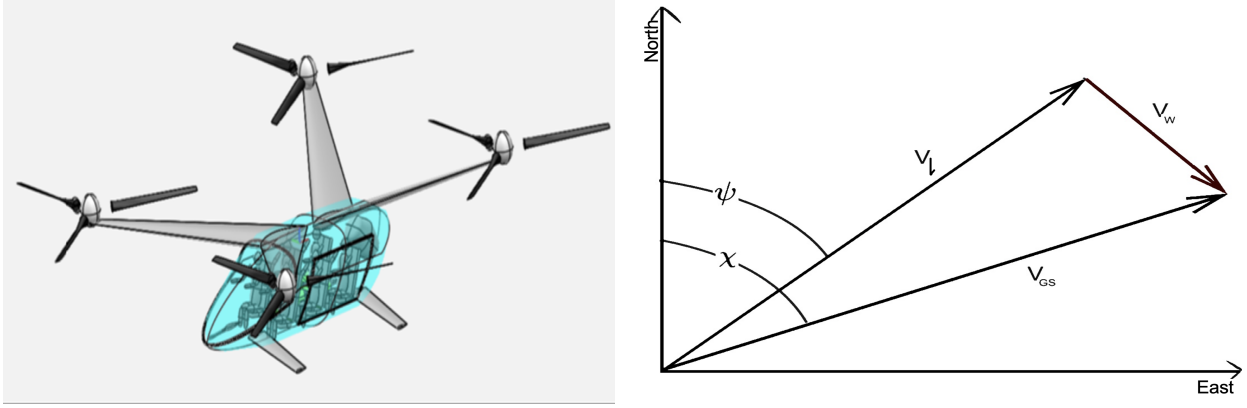

(a) Quadrotor eVTOL aircraft [4] **(b) Lateral navigation definition [5]**

Fig. 1 Multirotor eVTOL aircraft in forward flight

A. Power Required and Energy Consumption

1. Flight Dynamics, Kinematics, Thrust and Drag Models

The following quasi-steady flight dynamics, flight kinematics, drag and thrust models are used for generating quadrotor eVTOL aircraft trajectories using East-North-Up coordinate system [6]:

$$\frac{dV_l}{dt} = \frac{T\cos\phi\sin\theta - D\cos\gamma}{m} \tag{1}$$

$$\frac{dV_v}{dt} = \frac{T\cos\phi\cos\theta - D\sin\gamma - mg}{m} \tag{2}$$

$$\frac{d\psi}{dt} = \frac{T\sin\phi}{mV_l} \tag{3}$$

$$\frac{d\lambda}{dt} = \frac{V_l\cos\psi + W_n}{(R_{\text{Earth}} + h)} = \frac{V_{GS}\cos\chi}{(R_{\text{Earth}} + h)} \tag{4}$$

$$\frac{d\tau}{dt} = \frac{V_l\sin\psi + W_e}{(R_{\text{Earth}} + h)\cos\lambda} = \frac{V_{GS}\sin\chi}{(R_{\text{Earth}} + h)\cos\lambda} \tag{5}$$

$$\frac{dh}{dt} = V_v + W_v \tag{6}$$

$$\tan\gamma = \frac{V_v}{V_l} \tag{7}$$

$$T = 4T_{\text{rotor}} \tag{8}$$

$$D = 1.1984q \tag{9}$$

where λ is the latitude, τ is the longitude, V_l is the lateral component of the true airspeed and ψ is the heading angle w.r.t north, h is the altitude, V_v is the vertical component of the true airspeed, T is the net thrust, $(T_{\text{rotor}})_n$ is the thrust produced by the n^{th} rotor, θ is the rotor tip path plane pitch angle and ϕ is the rotor tip path plane roll (bank) angle, m is the mass of the aircraft, D is the parasite drag, q is the dynamic pressure, V_{GS} is the groundspeed, χ is the course, h is the altitude above mean sea level, R_{Earth} is the mean radius of the Earth, γ is the aerodynamic flight path angle, and W_e, W_n and W_v are the components of the wind in the east, north and vertical (up) directions, respectively.

2. Power Model

The instantaneous power required in forward flight is equal to the sum of the induced power, parasite power, climb power and profile power as follows [5–8]:

$$P_{\text{required}} = P_{\text{induced}} + P_{\text{parasite}} + P_{\text{climb}} + P_{\text{profile}} \tag{10}$$

$$P_{\text{required}} = \kappa \sum_{n=1}^{4} (T_{\text{rotor}} v_i)_n + TV \sin\alpha + \frac{\rho A_{\text{rotor}} (\omega R)^3 \sigma C_{d\ mean} F_P}{8} \tag{11}$$

where v_{i} is the induced velocity, κ is the induced power correction factor, α is the angle of attack between the air-stream and the rotor disk (tip path plane), V is the true airspeed of the aircraft, $C_{\text{d mean}}$ is the mean blade drag coefficient, σ is the thrust weighted solidity ratio, R is the radius of the rotor and F_{P} is the function that accounts for the increase of the blade section velocity with rotor edgewise and axial speed [4, 5]. The induced velocity (v_{i}) is numerically computed as described in [5]. The $C_{\text{d mean}}$ and κ are numerically computed as a function of the advance ratio (μ) as defined in [6].

3. Trajectory Generator

Great-circle trajectories are generated using the point mass model (Equations: 1 - 6) and great-circle navigation law [9] that employs thrust (T), rotor-tip path plane pitch (θ) and bank (ϕ) angles as controls. The equations of motion are integrated forward in time using the controls needed for following the desired lateral path and vertical path (climb, cruise, and descent) [9]. The performance data of the eVTOL aircraft used in this research is from [4, 6].

4. Motor Control and Energy Consumption

Thrust is controlled by using the collective pitch to change the pitch of the propeller blade. A detailed study by Malpica et'al [10] presents a design of the flight control system for electric propulsion of quad-rotor configurations of varying gross weight using variable collective blade pitch control. The design was informed by conceptual model parameters. Variable collective blade pitch method is selected for control because inertia of the propeller rotor with the gearbox makes angular velocity (rotations-per-minute (rpm)) control difficult.

As discussed in Ref. [11], angular velocity control is not practical for good handling quality and disturbance rejection due to the inertia effect. Propulsion is therefore provided by using constant rpm electric motors; the current is changed for achieving the torque required for maintaining the constant rpm as the blade pitch is altered.

IV. Experimental Setup

A. MACCOR Battery Tester

The Series 4000 MACCOR Battery Tester system, shown in Fig.2, consists of a test cabinet, a computer and software for the tester and data analysis. The test cabinet, with its embedded microprocessors, and the computer are connected together in a 10-Base-T Local Area Network (LAN). The embedded microprocessor controller boards control the tests and collect data. Each controller supports from one to eight test channels. The test cabinet also contains the individually controllable programmable loads and power supplies. Each test channel can be operated independently, which enables simultaneous testing of different tests. The operator programs the tests on the computer using a menu-driven Graphical User Interface. The programmed test is downloaded to the target channel's embedded controller board on initiation of the test.The controller board controls the test parameters and collects data. The measured data are transferred to the computer for storage and analysis when the programmed test end condition is reached.

If testing is desired in a temperature controlled environment, the battery is placed inside a thermal chamber such as the one shown in Fig.3. This figure shows the Tenney Thermal Product Solutions (TPS) lab vacuum oven, which is designed for drying, curing, aging, process control and other applications requiring elevated temperature in reduced atmospheres. Battery temperature rises as more current is drawn by the load. The chamber enables simulation of the battery operating conditions by either letting the temperature increase and decrease as a function of current drawn, or heating and cooling to maintain the specified temperature. In this research, the battery temperature was maintained at 25 degrees Celsius. The wires inside the thermal chamber, attached to the battery, are connected to the MACCOR tester for performing the tests.

In the electrical cycling characterization procedure, cells and packs are subjected to the charge/discharge profiles expected in flight. The MACCOR Battery tester system is programmed to run a similar power demand profile as in the simulated trajectory for analysis of the battery performance.

Fig. 2 MACCOR Battery Tester - Experimental Setup

The battery packs are subjected to different operating conditions to test the safety mechanisms under adverse conditions. The steps for preparing the battery cells for the experiment are as follows:

- Battery pack is charged at 1C of the rate current
- Discharge the battery pack based on the flight power profile as shown in Tables.3 and 2 generated through the discussion in Section III.A.1
- This profile is normalized to the ratings of the battery under test.
- Record current, voltage and temperature during the cycles are recorded through the MACCOR test unit.

For this work, performance of the battery at different cruise C rates is planned at constant temperature.
C rating means. what does changing of C rates does to the battery SOC and distance travelled.

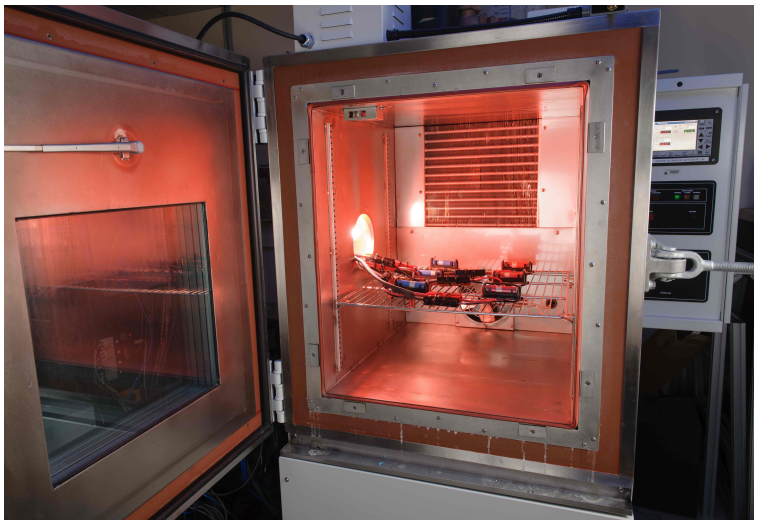

Fig. 3 Environmental Chamber for Testing Batteries

B. Electro-Chemistry Based Battery Model

The electro-chemistry (EC) based model of Li-Po battery pack developed by Daigle and Kulkarni [12] is used in this research. This model captures the significant electrochemical processes, and it reliably predicts state-of-charge (SOC) and end-of-discharge (EOD). This model and prognostics algorithms have been verified and validated on electric UAV's in earlier research [13].

C. Simulation Setup

The nominal speed is assumed to be 43 m/s (about 84 knots) for a 30 nm flight. The power consumption of 144 kW, by the vehicle at this speed is then normalized with the rest of the flight profiles and to a single cell in a battery pack. The model is generalized for different battery pack sizes and can be modified with additional information of the pack size for future studies.

Energy profiles generated from the simulation data [6] are scaled down to a single 22Ah Lithium-polymer (Li-po) battery pack. Tattu Plus 22000mAh 6S1P Lipo Battery Pack are being used for the hardware simulation experiments. The rating 22000Ah indicates the battery can support 22A constant current being drawn for a period of one hour. This number is the C rate of the battery pack i.e 1C = 22A. In the current scenario, these battery packs are well suited for electric UAV vehicles like DJI S1000, S1000+ and Tarot T8, which are amongst the current vehicles being used for performing battery algorithm development within the group [13].

The scaling down of energy from vehicle to a single pack is based on [4], where in Table III, "Comparison of Concept Vehicle Attributes," in this reference, the Cruise C-rate (1/hr) is assumed to be 0.6 C for the discussed eVTOL vehicles. Energy values calculated and discussed in [6] are also based on the same vehicle types. Based on this, the values from the simulated flight trajectory are normalized to the selected 6S1P battery pack and simulated experimentally in the MACCOR tester.

As discussed in Section III.A.4, power draw is based on varying the current which is similar to the approach discussed in [11] of collective control at constant rotor rpm.

Table 1 Power required (kW) in different phases of flight of a simulated 30 nm flight of eVTOL aircraft

Cruise Altitude (m)	Power Required (kW)					
	Vertical Takeoff	Climb	Cruise	Descent (45 Deg)	Approach (8 Deg)	Vertical Landing
500	264.94	273.53	142.74	Negligible	Negligible	139.45
1000	264.94	272.66	148.10	Negligible	Negligible	139.45
2000	264.94	273.03	154.84	Negligible	Negligible	139.45
3000	264.94	273.13	161.54	Negligible	Negligible	139.45

Table 1 shows power drawn (KW) in the different phases of the 30 nm eVTOL flight. The phases of flight include vertical takeoff, climb, cruise, approach and vertical landing. The time spent in the phases of flight are listed in Table 2. The total energy drawn from the batteries is directly proportional to the time spent in each phase. Our study assumes all external affecting conditions remain constant. Our study also did not consider energy optimization for the simulated flight, which could be expected to affect the flight trajectory, therefore, the time spent in the different phases of flight.

Table 2 Duration (in seconds) of the different phases of simulated 30 nm eVTOL flight

Cruise Altitude (m)	Flight Duration (sec)					
	Vertical Takeoff	Climb	Cruise	Descent (45 Deg)	Approach (8 Deg)	Vertical Landing
500	15.51	85	680.8	0	115	15.5
1000	15.51	180	855.5	11.4	115	15.5
2000	15.51	369	1045.9	32.6	115	15.5
3000	15.51	558	1147.9	52.1	115	15.5

Table 3 shows the normalized power values for the single battery pack following the procedure in [4]. The normalized power values in Table 3 and flight time in Table 2 are used for generating the battery pack load as a function of time.

Table 3 Normalized power drawn (W) from the 6S1P battery pack in different phases of the 30 nm flight for simulation in the MACCOR

Cruise Altitude (m)	Normalized Power Drawn (W)					
	Vertical Takeoff	Climb	Cruise	Descent (45 Deg)	Approach (8 Deg)	Vertical Landing
500	607.28	628.75	328.12	0	0	320.56
1000	607.52	626.76	340.43	0	0	320.56
2000	607.52	627.61	355.94	0	0	320.56
3000	607.52	627.84	371.32	0	0	320.56

V. Results and Discussion

A. Flight Phases

In this study, the trajectory of the eVTOL aircraft is divided into six distinct flight phases, i.e., vertical takeoff, climb, cruise, descent, approach, and vertical landing. Each of the flight phase is discussed as follows:

- Vertical takeoff phase involves vertical climb from MSL to 15 m AGL at an acceleration of 0.2g m/s^2. The average power required in this flight phase is 264.29 kW, and the flight duration is 15.5 seconds.
- Climb phase involves shallow climb at 10-degree flight path angle at the maximum endurance airspeed (30 m/s) as the lateral component of the airspeed [6] until reaching the cruise altitude. The computed average power required in the climb phase is 273.5 kW, and the flight duration is a function of the cruise altitude.
- Cruise phase involves flying at a constant altitude at the best-range airspeed [14]. The average power required is a function of the cruise altitude as shown in Table 4.
- Descent phase involves descent at 45 degrees flight path angle at the best-range airspeed. The descent phase consists of descending from the cruise altitude to 500 m AGL. The average power required in this flight phase turned out to be negligible given steep descent flight path angle (45 deg), and best-range airspeed [15]. In the descent flight phase, for the given flight path angle and airspeed, the power required is negligible as energy is supplied by the surrounding air. Also, observed: (i) the component of the airspeed normal to the rotor tip-path-plane (V$\sin\alpha$) is less than negative two times rotor induced velocity in hover (v_h), and (ii) the component of the airspeed parallel to the rotor tip-path-plane (V$\cos\alpha$) is greater than four times rotor induced velocity in hover (v_h) [8].
- Approach phase involves descending at 8 degrees flight path angle at the maximum endurance airspeed. The average power required computed in the approach flight phase also turned out to be negligible. In the approach flight phase, for the given flight path angle and airspeed, the power required is negligible as energy is supplied by the surrounding air. Also, observed: (i) the component of the airspeed normal to the rotor tip-path-plane (V$\sin\alpha$) is less than negative one-half times rotor induced velocity in hover (v_h), and (ii) the component of the airspeed parallel to the rotor tip-path-plane (V$\cos\alpha$) is greater than three times rotor induced velocity in hover (v_h) [8].
- Vertical landing phase involves descending vertically from 15 m AGL to MSL at a deceleration of 0.2g m/s^2. The average power required and the flight duration in this flight phase are computed to be 139.45 kW and 15.5 seconds, respectively.

The power required and energy consumption during the transition between the flight phases have been ignored in this study.

Table 4 Cruise Flight Phase [6, 14]

Cruise Altitude (m)	Best-Range Airspeed (m/s)	Power Required (kW)
500	43	142.74
1000	44	148.10
2000	46	154.84
3000	48	161.54

B. Simulated Flight Profiles

This section discusses battery discharge profile for a simulated flight where power drawn is normalized for a 6S 22Ah battery pack. This experimental condition assumes that the power drawn at cruise speed mode is 0.6C of the rated battery as discussed in Section IV.C.

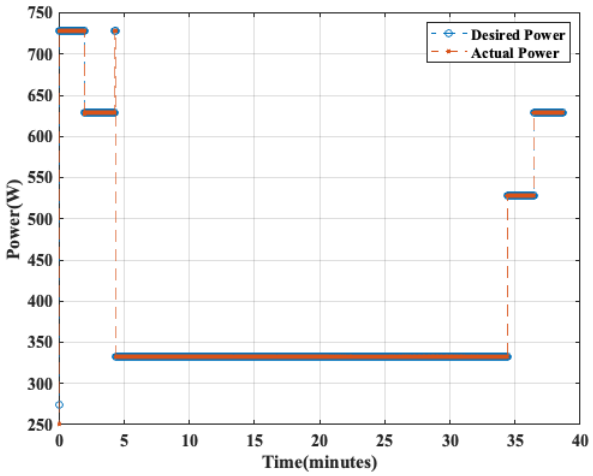

Fig. 4 Flight Profile Simulation on a Li-Po 6S Battery Pack with normalized power draw comparing desired power from the simulation and actual power drawn from the MACCOR tester

The plot in Fig. 4 shows the comparison of actual power draw vs normalized power draw. The power draw is considerably high during first two phases of the flight i.e vertical takeoff, climb. During the cruise phase it is minimal which is equivalent to the 0.6C discharge rate. The power draw increases in the subsequent flight phases.

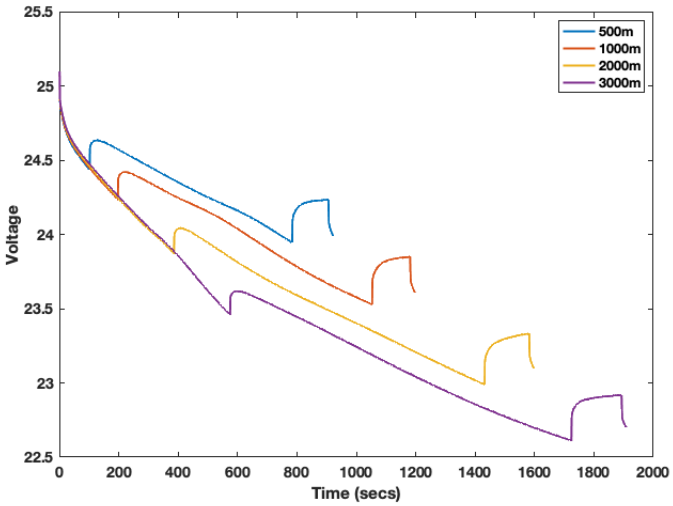

Fig. 5 Voltage Discharge Plots : Flight Profile Simulation on a Li-Po 6S Battery Pack at 4 different altitudes for 30 nm range as discussed in Table3

Fig. 5 shows the voltage plots for the four simulated flight profiles as discussed in Table 2 with the Li-Po battery pack. Based on the variation in the power draw, it is observed that voltage drops in the early flight phases due to high power required for vertical lift and climb to cruise altitude. The voltage decreases linearly in the cruise phase. A jump in the voltage is observed during the decent and approach phases because the motors do not draw power from the batteries in these phases. The voltage drops during vertical landing as shown in the plots.

Because the simulation was being conducted at single pack level, a vehicle level pack was assumed with 10 series and 50 parallel (10S50P) configuration shown in Fig.6. Though this is not the exact configuration for the vehicle, the authors used this hypothesized configuration to demonstrate and help readers visualize vehicle level voltage and current behaviour.

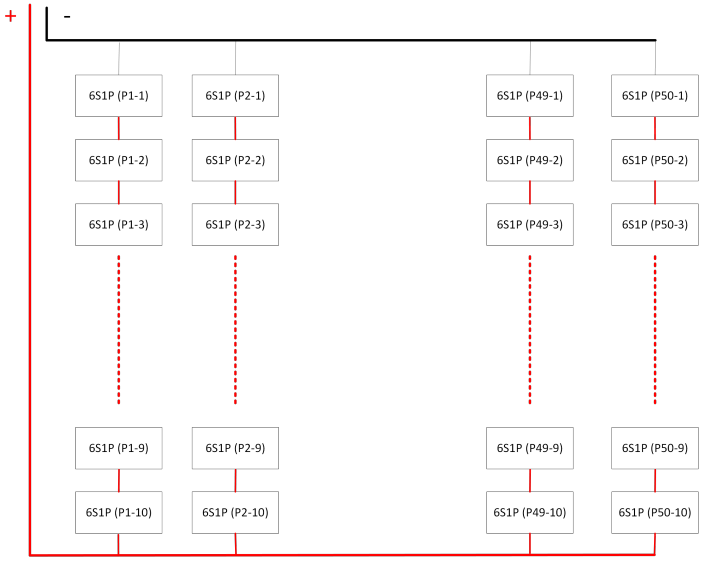

Fig. 6 10S50P Pack level schematic configuration

Fig. 7 shows the 10S50P pack voltage discharge profiles with reference to the four altitude profiles for the 30 nm flight. The voltage discharge plots provide a better understanding of remaining charge present in the battery pack at the end of the each 30 nm flight flown at a different cruise altitude.

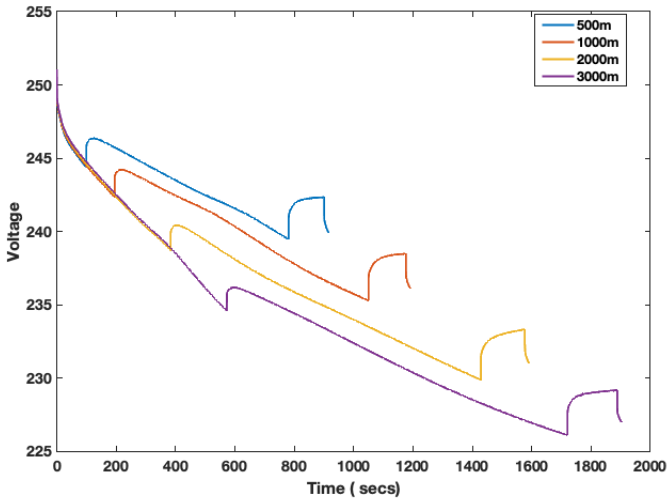

Fig. 7 Voltage Discharge Plot : Profile Simulation at vehicle level with for four different altitudes for 30 nm range as discussed in Table 2

VI. Conclusions

The purpose of this research study was to determine battery pack requirements for providing the power required for flying a multirotor electric vertical takeoff and landing aircraft for 30 nm at different cruise airspeeds corresponding to the different cruise altitudes with an adequate margin of safety (battery pack does not discharge below the specified threshold).

A NASA-proposed conceptual multirotor electric vertical takeoff and landing aircraft was used for the simulated flights in the urban environment to estimate the power required using the flight kinematics, flight dynamics, and aircraft performance data. The power required by the multirotor aircraft was determined for various flight phases of 30 nm range flights. The flights were simulated to cruise at different altitudes such as 500, 1000, 2,000, and 3,000 m. The cruise airspeed current draw is assumed to be 0.6C. The calculated power required for the simulated trajectories was normalized to 6S1P Lithium-polymer battery packs. The battery packs were tested in the laboratory using a MACCOR battery tester.

Through this study, the authors demonstrated a hardware-in-loop procedure to simulate the performance of a battery pack for providing the propulsion needs of a multirotor electric takeoff and landing aircraft. The results show the power draw and voltage drop for flying the aircraft at airspeeds corresponding to different cruise altitudes. The multirotor aircraft flight at higher cruise altitudes leads to higher voltage discharge and lower state-of-charge.

The authors plan to perform hardware-in-loop experiments to estimate battery performance in terms of voltage discharge and state-of-charge at different C rates for simulated flights at different cruise airspeeds corresponding to different cruise altitudes in the future.

Further, the model based prognostics framework will be implemented to estimate the state-of-charge as well as to predict the remaining flight time based on the allowable discharge threshold for the given flight profile.

Acknowledgments

The work by Gano Chatterji and Priyank Pradeep is funded by NASA's Aeronautics Research Mission Directorate through the Revolutionary Vertical Lift Technology Project of the Advanced Air Vehicle Program.

The work by Chetan Kulkarni was supported by the System-Wide Safety (SWS) project under the Airspace Operations and Safety Program within the NASA Aeronautics Research Mission Directorate (ARMD) and under NASA Ames Research Center, Contract No. 80ARC020D0010.

References

[1] Bosson, C., and Lauderdale, T. A., "Simulation evaluations of an autonomous urban air mobility network management and separation service," *2018 Aviation Technology, Integration, and Operations Conference*, 2018, p. 3365. doi:10.2514/6.2018-3365.

[2] Pradeep, P., and Wei, P., "Energy-efficient arrival with rta constraint for multirotor evtol in urban air mobility," *Journal of Aerospace Information Systems*, Vol. 16, No. 7, 2019, pp. 263–277.

[3] Thipphavong, D. P., Apaza, R., Barmore, B., Battiste, V., Burian, B., Dao, Q., Feary, M., Go, S., Goodrich, H. J., Kenneth H, Idris, H. R., Kopardekar, P. H., Lachter, J. B., Neogi, N. A., Ng, H. K., Oseguera-Lohr, R. M., Patterson, M. D., and Verma, S. A., "Urban air mobility airspace integration concepts and considerations," *2018 Aviation Technology, Integration, and Operations Conference*, 2018, p. 3676. doi:10.2514/6.2018-3676.

[4] Silva, C., Johnson, W. R., Solis, E., Patterson, M. D., and Antcliff, K. R., "VTOL Urban Air Mobility Concept Vehicles for Technology Development," *2018 Aviation Technology, Integration, and Operations Conference*, 2018, p. 3847.

[5] Pradeep, P., Lauderdale, T. A., Chatterji, G. B., Sheth, K., Lai, C. F., Sridhar, B., Edholm, K.-M., and Erzberger, H., "Wind-Optimal Trajectories for Multirotor eVTOL Aircraft on UAM Missions," *AIAA AVIATION 2020 FORUM*, 2020, p. 3271.

[6] Pradeep, P., Kulkarni, C. S., Chatterji, G. B., and Lauderdale, T. A., "Parametric Study of State-of-Charge for an Electric Aircraft in Urban Air Mobility," *AIAA AVIATION 2021 FORUM*, 2021.

[7] Johnson, W., Silva, C., and Solis, E., "Concept Vehicles for VTOL Air Taxi Operations," *Conference on Aeromechanics Design for Transformative Vertical Flight, San Francisco, CA*, 2018.

[8] Johnson, W., *Helicopter theory*, Courier Corporation, 2012.

[9] Chatterji, G. B., "Trajectory Simulation for Air Traffic Management Employing a Multirotor Urban Air Mobility Aircraft Model," *AIAA AVIATION 2020 FORUM*, 2020, p. 3209. doi:10.2514/6.2020-3209, URL `https://arc.aiaa.org/doi/abs/10.2514/6.2020-3209`.

[10] Malpica, C. A., "Handling Qualities Analysis of Blade Pitch and Rotor Speed Controlled eVTOL Quadrotor Concepts for Urban Air Mobility," 2020.

[11] Tallerico, T., *NASA Reference Motor Designs for Electric Vertical Takeoff and Landing Vehicles*, ???? doi:10.2514/6.2021-3279, URL https://arc.aiaa.org/doi/abs/10.2514/6.2021-3279.

[12] Daigle, M., and Kulkarni, C., "Electrochemistry-based Battery Modeling for Prognostics," *Annual Conference of the Prognostics and Health Management Society 2013*, 2013, pp. 249–261.

[13] Hogge, E., Bole, B., Vazquez, S., Kulkarni, C., Strom, T., Hill, B., Smalling, K., and Quach, C., "Verification of Prognostic Algorithms to Predict Remaining Flying Time for Electric Unmanned Vehicles," *International Journal of Prognostics and Health Management, ISSN 2153-2648, 2018 021*, 2018.

[14] Pradeep, P., Lauderdale, T. A., Erzberger, H., and Chatterji, G. B., "Wind-Optimal Cruise Airspeed for a Multirotor Aircraft in Urban Air Mobility," 2022. doi:10.2514/6.2022-0262, URL https://arc.aiaa.org/doi/abs/10.2514/6.2022-0262.

[15] Johnson, W., "Helicopter optimal descent and landing after power loss," 1977.